

## LJMU Research Online

**Saracino, S, Martocchia, S, Bastian, N, Kozhurina-Platais, V, Chanterreau, W, Salaris, M, Cabrera-Ziri, I, Dalessandro, E, Kacharov, N, Lardo, C, Larsen, SS and Platais, I**

**Chromosome maps of young LMC clusters: An additional case of coeval multiple populations**

<http://researchonline.ljmu.ac.uk/id/eprint/12499/>

### Article

**Citation** (please note it is advisable to refer to the publisher's version if you intend to cite from this work)

**Saracino, S, Martocchia, S, Bastian, N, Kozhurina-Platais, V, Chanterreau, W, Salaris, M, Cabrera-Ziri, I, Dalessandro, E, Kacharov, N, Lardo, C, Larsen, SS and Platais, I (2020) Chromosome maps of young LMC clusters: An additional case of coeval multiple populations. Monthly Notices of the Royal**

LJMU has developed **LJMU Research Online** for users to access the research output of the University more effectively. Copyright © and Moral Rights for the papers on this site are retained by the individual authors and/or other copyright owners. Users may download and/or print one copy of any article(s) in LJMU Research Online to facilitate their private study or for non-commercial research. You may not engage in further distribution of the material or use it for any profit-making activities or any commercial gain.

The version presented here may differ from the published version or from the version of the record. Please see the repository URL above for details on accessing the published version and note that access may require a subscription.

For more information please contact [researchonline@ljmu.ac.uk](mailto:researchonline@ljmu.ac.uk)

<http://researchonline.ljmu.ac.uk/>



# Chromosome maps of young LMC clusters: an additional case of coeval multiple populations

S. Saracino<sup>1</sup>,<sup>1</sup>★ S. Martocchia,<sup>1,2</sup> N. Bastian,<sup>1</sup> V. Kozhurina-Platais,<sup>3</sup> W. Chantreau,<sup>1</sup> M. Salaris,<sup>1</sup> I. Cabrera-Ziri,<sup>4</sup>† E. Dalessandro,<sup>5,9</sup> N. Kacharov,<sup>6</sup> C. Lardo<sup>7</sup>, S. S. Larsen<sup>8</sup> and I. Platais<sup>10</sup>

<sup>1</sup>Astrophysics Research Institute, Liverpool John Moores University, 146 Brownlow Hill, Liverpool L3 5RF, UK

<sup>2</sup>European Southern Observatory, Karl-Schwarzschild-Straße 2, D-85748 Garching bei München, Germany

<sup>3</sup>Space Telescope Science Institute, 3700 San Martin Drive, Baltimore, MD 21218, USA

<sup>4</sup>Harvard-Smithsonian Center for Astrophysics, 60 Garden Street, Cambridge, MA 02138, USA

<sup>5</sup>INAF – Osservatorio di Astrofisica and Scienza dello Spazio, via Gobetti 93/3, I-40129 Bologna, Italy

<sup>6</sup>Max-Planck-Institut für Astronomie, Königstuhl 17, D-69117 Heidelberg, Germany

<sup>7</sup>Laboratoire d'astrophysique, École Polytechnique Fédérale de Lausanne (EPFL), Observatoire, CH-1290 Versoix, Switzerland

<sup>8</sup>Department of Astrophysics/IMAPP, Radboud University, P.O. Box 9010, NL-6500 GL Nijmegen, The Netherlands

<sup>9</sup>Dipartimento di Fisica and Astronomia, Università degli Studi di Bologna, via Gobetti 93/2, I-40129 Bologna, Italy

<sup>10</sup>Department of Physics and Astronomy, Johns Hopkins University, 3400 North Charles Street, Baltimore, MD 21218, USA

Accepted 2020 February 27. Received 2020 January 22; in original form 2019 November 27

## ABSTRACT

Recent studies have revealed that the multiple populations (MPs) phenomenon does not occur only in ancient and massive Galactic globular clusters (GCs), but it is also observed in external galaxies, where GCs sample a wide age range with respect to the Milky Way. However, for a long time, it was unclear whether we were looking at the same phenomenon in different environments or not. The first evidence that the MPs phenomenon is the same regardless of cluster age and host galaxy came out recently, when an intermediate-age cluster from the Small Magellanic Cloud, Lindsay 1, and a Galactic GC have been directly compared. By complementing those data with new images from the *Hubble Space Telescope* (*HST*), we extend the comparison to two clusters of different ages: NGC 2121 ( $\sim 2.5$  Gyr) and NGC 1783 ( $\sim 1.5$  Gyr), from the Large Magellanic Cloud. We find a clear correlation between the RGB (red giant branch) width in the pseudo-colour  $C_{F275W, F343N, F438W}$  and the age of the cluster itself, with the older cluster having larger  $\sigma(C_{F275W, F343N, F438W})^{\text{RGB}}$  and vice versa. Unfortunately, the  $\sigma$  values cannot be directly linked to the N-abundance variations within the clusters before properly taking account the effect of the first dredge-up. Such *HST* data also allow us to explore whether multiple star formation episodes occurred within NGC 2121. The two populations are indistinguishable, with an age difference of only  $6 \pm 12$  Myr and an initial helium spread of 0.02 or lower. This confirms our previous results, putting serious constraints on any model proposed to explain the origin of the chemical anomalies in GCs.

**Key words:** techniques: photometric – galaxies: individual: LMC, SMC – galaxies: star clusters: individual: Lindsay 1, NGC 2121, NGC 1783.

## 1 INTRODUCTION

Globular clusters (GCs) are no longer considered the best example of single stellar populations (SSP), since much observational evidence has shown that they host star-to-star abundance variations in terms of light elements (e.g. C, N, O, and Na). The multiple

populations (MPs) phenomenon has been extensively studied in the last years, coming to the conclusion that it is not a peculiarity of Milky Way (MW) GCs but it can be also found in star clusters belonging to external galaxies: Magellanic Clouds (MCs, Mucciarelli et al. 2009; Milone et al. 2009; Dalessandro et al. 2016; Niederhofer et al. 2017a; Gilligan et al. 2019), Fornax dwarf (Larsen et al. 2014), and Sagittarius dwarf galaxies (e.g. M54, Carretta et al. 2010; Sills et al. 2019). This finding immediately ruled out the host environment as one of the key elements to understand the phenomenon. Together with mass (Carretta et al. 2010; Bragaglia

★ E-mail: s.saracino@ljmu.ac.uk

† Hubble Fellow

et al. 2012; Schiavon et al. 2013; Milone et al. 2017), age plays a crucial role in defining the (observable) onset and properties of chemical anomalies. In the recent years, in fact, MPs have been detected in almost all ancient clusters surveyed (Milone et al. 2015, 2017), as well as in intermediate-age clusters (Hollyhead et al. 2017; Niederhofer et al. 2017a,b; Martocchia et al. 2018a,b, 2019; Milone et al. 2019), disappearing for clusters younger than  $\sim 2$  Gyr (Martocchia et al. 2017).

The mechanism that triggers the presence of MPs in GCs is still unknown and under debate but its understanding may have important implications for the assembly history of galaxies hosting GC systems (e.g. Bastian & Lardo 2018). Several scenarios have been proposed over the years but we still lack a theory able to explain all the recent observational findings. Indeed, depending on the source of the chemical enrichment within the cluster, many theories proposed so far predict age spreads ranging from a few Myr (massive and supermassive stars, e.g. Decressin et al. 2007; Denissenkov & Hartwick 2014; Gieles et al. 2018) up to 30–200 Myr [asymptotic giant branch (AGB) stars, e.g. D’Ercole et al. 2008; Conroy & Spergel 2011]. An efficient way to rule out one or the other scenarios would be to estimate the age difference among the subpopulations in a cluster. A first attempt in this direction has been done by Marino et al. (2012) and Nardiello et al. (2015), where the authors found only upper limits of  $\sim 200$  Myr, since they focused on ancient GCs. Martocchia et al. (2018b) repeated the experiment for the  $\sim 2$  Gyr cluster NGC 1978 in the Large Magellanic Cloud (LMC), finding an age difference of  $1 \pm 20$  Myr between the two populations: such a result appears to impose a stringent constraint on the onset of MPs.

This work is the second in a series aimed at investigating the MPs phenomenon in LMC/SMC (Small Magellanic Cloud) clusters through specific diagnostics (e.g. the so-called chromosome map by Milone et al. 2017), which have been designed for MW GCs but can now be applied to explore different regimes. In Saracino et al. (2019b), we took advantage of new ultraviolet (UV) data acquired under our ongoing *Hubble Space Telescope* (HST) survey of LMC/SMC massive clusters, to make the first direct comparison between the SMC intermediate-age cluster Lindsay 1 and the Galactic GC NGC 288, by demonstrating that the MPs formation mechanism should be the same for different galaxies, as well as at different GCs ages. Here, we complement those data with that of two young clusters, namely NGC 2121 and NGC 1783 from the LMC, to analyse in detail how the MPs phenomenon changes with the cluster age. Then we focus our attention on NGC 2121, in order to determine the possible helium (He) enrichment within the cluster, as well as the possible age difference between its sub-populations.

This paper is organized as follows: in Section 2, the observational data base, the photometric reduction and the analysis are presented. In Section 3, an alternative diagnostic for MPs is used to compare Lindsay 1, NGC 2121, and NGC 1783. In Section 4, we discuss the presence of He-abundance variations in NGC 2121. The analysis of its sub giant branch (SGB) is then presented in Section 5. We finally summarize the most relevant results and draw our conclusions in Section 6.

## 2 OBSERVATIONS AND DATA ANALYSIS

### 2.1 Data and photometry

The observations of the three clusters analysed in this work, namely Lindsay 1, NGC 2121 and NGC 1783, are from HST

and they consist in both proprietary and archival data from our group, covering a wide wavelength range. In particular, the F336W, F343N, and F438W filters come from the HST survey of LMC/SMC star clusters performed in the last years using the WFC3/UVIS camera (proposals GO-14069 and GO-15062; PI: N. Bastian). These observations have been recently complemented with new data in the UV filter F275W, under the proposal GO-15630 (PI: N. Bastian). For NGC 2121, even the F814W images have been collected under this ongoing HST program. For the other two clusters, we took advantage of archival data from the Advanced Camera for Surveys (ACS) in the F814W filter. In particular, the data for Lindsay 1 come from the program GO-10396, PI: J. Gallagher, while the data for NGC 1783 have been acquired under the program GO-10595 (PI: P. Goudfroijj). The main properties of the WFC3/UVIS and ACS/WFC images used in the paper, in terms of exposure times in the different filters, are summarized in Table 1. We also point out that the data for Lindsay 1 have not been reduced for this paper, since we used the photometric catalog recently published by Saracino et al. (2019b).

The photometric analysis has been performed with DAOPHOT IV (Stetson 1987) on images processed, flat-fielded, bias-subtracted, and corrected for charge transfer efficiency losses by standard HST pipelines (*\_flc* images). As a first step, few hundreds of stars have been selected in each image and chip in order to model the point spread function (PSF), by considering a 10-pixel aperture. The PSF models were chosen on the basis of a  $\chi^2$  statistic and, in average, the best fit has been provided by a Moffat function (Moffat 1969). These models were finally applied to all the sources detected at more than  $3\sigma$  from the background level in each image. Then, we built a master catalogue with stars detected in at least half the available images per filter. In some cases, a less restrictive criterion has been adopted in order to cover the gap between the two chips. At the corresponding positions of these stars, the photometric fit was forced in all the other frames by using DAOPHOT IV/ALLFRAME (Stetson 1994). Finally, the magnitude and photometric error of each star has been estimated as the weighted mean and standard deviation of those measured in multiple images.

Instrumental magnitudes have been then reported to the VEGA-MAG system by using the zero-points values quoted both in the WFC3 and ACS websites (at the aperture size), as well as appropriate aperture corrections at a radius of 10 pixels from the stellar centres. Instrumental positions have been reported to the absolute coordinate system (RA, Dec.) by using the stars in common with the *Gaia* Data Release 2 (DR2, *Gaia* Collaboration et al. 2016, 2018) and by means of the cross-correlation software CATAXCORR (Montegriffo et al. 1995). This software has been also used to combine the final WFC3 and ACS catalogues of the clusters.

### 2.2 Background decontamination and differential reddening

From previous studies of LMC/SMC clusters (e.g. Dalessandro et al. 2019), we have learned that the contamination from field stars could be relevant in these regions, contributing in some way to alter the scientific results. It appears to be not the case for Lindsay 1, where the contribution is relatively low (Saracino et al. 2019b). For NGC 2121 and NGC 1783, we instead adopted a statistical approach, which allows to estimate the fraction of star interlopers along the main evolutionary sequences in a colour–magnitude diagram (CMD). In particular, we applied the method described by Cabrera-Ziri et al. (in preparation), which has already been successfully tested on the SMC cluster NGC 419. This method is similar to the

**Table 1.** Main properties of the archival and proprietary *HST* images for Lindsay 1, NGC 2121, and NGC 1783 used in the paper.

Cluster	Instrument	Filter	Date	N×Exposure time	Proposal	PI
Lindsay 1	UVIS/WFC3	F275W	2019	1500s+1501s+2 × 1523s+2 × 1525s	15630	N. Bastian
	UVIS/WFC3	F336W	2011	500s+2 × 1200s	14069	N. Bastian
	UVIS/WFC3	F343N	2016	500s+800s+1650s+1850s	14069	N. Bastian
	UVIS/WFC3	F438W	2016	120s+2 × 460s	14069	N. Bastian
	WFC/ACS	F814W	2006	10s+4 × 474s	10396	J. Gallagher
NGC 2121	UVIS/WFC3	F275W	2019	1501s+1511s+1512s+1519s+1521s + 4 × 1523s+1525 + 2 × 1529s	15630	N. Bastian
	UVIS/WFC3	F336W	2011	270s+2 × 715s	15062	N. Bastian
	UVIS/WFC3	F343N	2016	450s+2 × 1250s+1650s	15062	N. Bastian
	UVIS/WFC3	F438W	2016	120s+2 × 550s	15062	N. Bastian
	UVIS/WFC3	F814W	2019	3 × 200s+3 × 350s+700s	15630	N. Bastian
NGC 1783	UVIS/WFC3	F275W	2019	2 × 1500s+4 × 1512s	15630	N. Bastian
	UVIS/WFC3	F336W	2011	2 × 1190s+1200s	12257	L. Girardi
	UVIS/WFC3	F343N	2016	450s+845s+1650s	14069	N. Bastian
	WFC/ACS	F435W	2006	90s+2 × 340s	10595	P. Goudfrooij
	WFC/ACS	F814W	2006	8s+2 × 340s	10595	P. Goudfrooij

one described by Niederhofer et al. (2017a) and commonly used in the previous papers of this series.

Since no parallel fields are available in the *HST* archive for NGC 2121 and NGC 1783, we then defined as cluster region, the first 40 arcsec (45 arcsec for NGC 1783) from the cluster centre,<sup>1</sup> while as control field region, the one made by all the stars located at a distance greater than 75 arcsec (80 arcsec for NGC 1783) from the centre. Since the area ratio between cluster and control field is  $\approx 0.6$ , for every star in the control region, we flagged  $\approx 0.6$  stars in the cluster region as likely members of the field according to its distance to the control field stars and the relative uncertainties. We repeated the same procedure 1000 times and at the end, we cleaned the cluster region by removing all the stars that have been flagged as field members > 75 per cent of the times. For a detailed description of the method we refer to Cabrera-Ziri et al. (in preparation).

The background subtraction procedure for NGC 2121 is presented as an example in Fig. 1. By comparing the cluster field with the decontaminated one (leftmost and rightmost panels, respectively), most of the stars lying on the blue of the MS (main sequence) have been rejected, as well as some spurious stars lying on the SGB and RGB (red giant branch) sequences, thus producing a much cleaner and more defined diagram. The output in the case of NGC 1783 is almost the same. The CMDs used in the rest of the paper refer to the innermost and background-subtracted portion of the clusters.

By inspecting the rightmost CMD of Fig. 1, it is clear that NGC 2121 is only slightly affected by differential reddening across the field of view (FOV) exploited in this study, since all the evolutionary sequences are very well defined. In Saracino et al. (2019b), the authors came to the same conclusions for Lindsay 1 and it appears to be quite common for such LMC/SMC clusters (Martocchia et al. 2018a, 2019). Anyway, we estimated the differential reddening effect in NGC 2121 and NGC 1783 in order to be consistent with

previous works. To do so, we used the method presented in Saracino et al. (2019a, see also Dalessandro et al. 2018). Briefly, we first created the cluster mean ridge line (MRL) in the  $(m_{F814W}, m_{F438W} - m_{F814W})$  CMD, then we selected a sample of bona-fide stars in the magnitude range  $19.5 < m_{F814W} < 22.5$  and we computed the geometrical distance ( $\Delta X$ ) of those stars from the MRL. This reference sample has been then used to assign a  $\Delta X$  value to each star in our photometric catalogue, by looking at its 30 closest reference stars. Using the extinction coefficients from Cardelli, Clayton & Mathis (1989), we finally transformed  $\Delta X$  of each star into the local differential reddening  $\delta E(B - V)$ . The resulting  $\delta E(B - V)$  are very low for both clusters (a mean value of 0.001 and a maximum variation of about 0.01 in the FOV), thus not producing any appreciable difference in their CMDs. As a double check, the technique explained in Milone et al. (2012) has been also used, coming to the same conclusions.

### 3 CHROMOSOME MAPS

One of the main tools adopted in the last years to look on to the MPs phenomenon in GCs is the so-called ‘chromosome’ map (Milone et al. 2017, 2018a), a pseudo-colour diagram which exploits a combination of F275W, F336W, F438W, and F814W filters to separate populations having different light-element abundances. The power of such a combination comes from two aspects: (1) the colour combination  $(m_{F275W} - m_{F814W})$  on the  $x$ -axis is mostly sensitive to temperature variations, and so to He-abundance variations among different stellar populations; and (2) the filter combination  $(m_{F275W} - m_{F336W}) - (m_{F336W} - m_{F438W}) = C_{F275W, F336W, F438W}$  on the  $y$ -axis is mainly a measure of the N-abundance variations within the cluster. The MPs phenomenon of Galactic GCs has been extensively investigated via the chromosome map in the last years thanks to the UV Legacy Survey of Galactic GCs (Piotto et al. 2015; Nardiello et al. 2018). It allowed the identification of, for example, the interesting trends between the light-elements enhancement in a cluster and its total mass. However almost all the GCs in the MW are essentially old (from 10 to 13 Gyr), thus representing one of the main limitations in putting all these findings in a more general framework. In this respect, the LMC/SMC survey of young- and intermediate-age clusters allowed us to investigate the phenomenon by looking into a different parameter space: the cluster age.

<sup>1</sup>The cluster centres of NGC 2121 and NGC 1783 have been determined by following the iterative procedure described in Montegriffo et al. (1995, see also Ferraro et al. 2003; Lanzoni et al. 2007), which consists in averaging the absolute positions of properly selected stars at different distances from a first-guess centre. (RA, Dec.) = (87.059036°, Dec. = −71.479805°) and (RA, Dec.) = (74.7880°, Dec. = −65.8965°) are the results for NGC 2121 and NGC 1783, respectively.



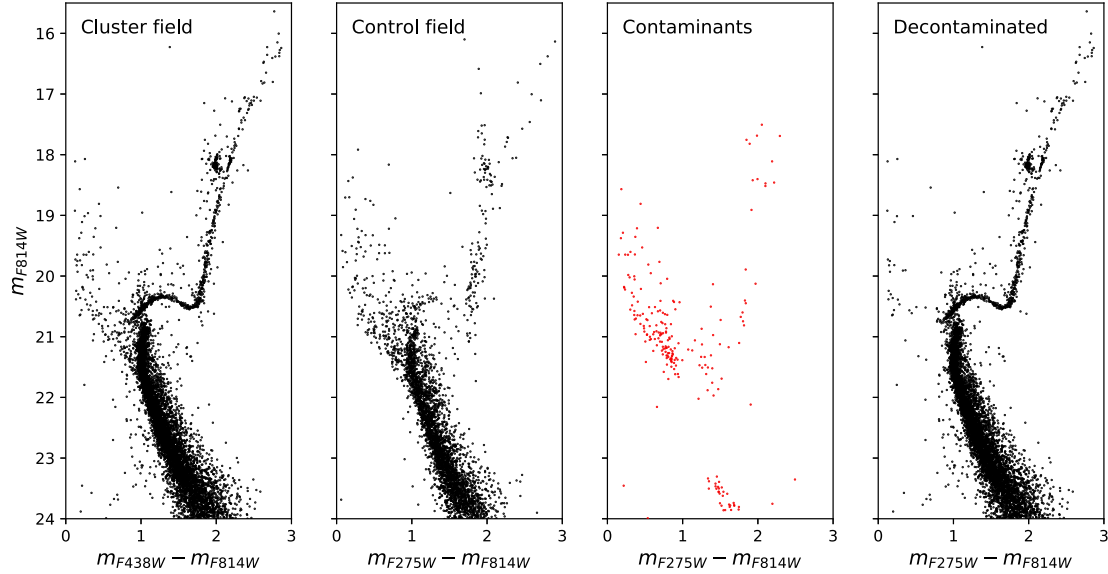


**Figure 1.** The first two panels represent the  $m_{F814W}$ ,  $m_{F438W} - m_{F814W}$  CMDs of the cluster region and the control field of NGC 2121 respectively, while the rightmost panel shows how the CMD of NGC 2121 looks like once the background decontamination is applied. The stars flagged as likely field members > 75 per cent of the times are shown in red in the figure and then removed from the final sample.

In particular, using a slightly different diagnostic, Martocchia et al. (2018a, 2019, see also Niederhofer et al. 2017a,b) have found a clear correlation between the N-enhancement and the cluster age, with no evidence of MPs for clusters younger than  $\sim 2$  Gyr. These studies have also demonstrated the power of the F343N filter of the WFC3/UVIS to infer the N-content of stars in clusters. A direct comparison of these two approaches has been recently performed in Saracino et al. (2019b), where we presented the first chromosome map of the extragalactic 7.5-Gyr old (Glatt et al. 2008) cluster Lindsay 1, demonstrating that they are both very effective methods for the detection of MPs in clusters. Here we complement the results achieved for Lindsay 1, with what derived for NGC 2121 and NGC 1783, having very different ages:  $\sim 2.5$  Gyr (Martocchia et al. 2019) and  $\sim 1.5$  Gyr (Cabrera-Ziri et al. 2016; Mucciarelli, Origlia & Ferraro 2007), respectively, by using a combined approach which exploits the power of the F343N filter in constructing the chromosome map of the clusters. This idea is also supported by fig. 3 of Milone et al. (2019), where the authors show that by substituting the F343N filter with the standard F336W, the distinction between the populations becomes even more pronounced. NGC 2121 has been discovered to host MPs by Martocchia et al. (2019, see also Li & de Grijs 2019), while NGC 1783 does not show any evidence of MPs from both photometric and spectroscopic studies (Mucciarelli et al. 2007; Cabrera-Ziri et al. 2016; Zhang et al. 2018).

To build the chromosome map of the three clusters, we have used the procedure outlined in Milone et al. (2017), but adopting the F343N filter instead of the F336W one. Briefly, we first used the  $(m_{F814W}, m_{F438W} - m_{F814W})$  CMD to select bona-fide RGB stars. Then we used the  $(m_{F814W}, m_{F275W} - m_{F814W})$  CMD to define two fiducial lines as the 5th and 95th percentiles of the  $(m_{F275W} - m_{F814W})$  distribution of the previously selected RGB stars. We then verticalized the distribution of RGB stars and normalized them to the intrinsic RGB width at 2 mag brighter than the turn-off in the F814W filter, thus creating the  $\Delta_{F275W, F814W}$ . The  $(m_{F814W}, m_{F275W} - m_{F814W})$  CMDs of the clusters are presented in Fig. 2, where the fiducial lines are highlighted in red and blue, in all the panels. We

applied the same approach to the pseudo-colour diagram  $(m_{F814W}, C_{F275W, F343N, F438W}^2)$ , in order to derive  $\Delta_{F275W, F343N, F438W}$ .

The pseudo  $(m_{F814W}, C_{F275W, F343N, F438W})$  CMDs of Lindsay 1, NGC 2121, and NGC 1783 are shown in Fig. 3, where the fiducial lines are colour-coded as in Fig. 2. These values have been used to compute the  $(\Delta_{F275W, F814W}$  versus  $\Delta_{F275W, F343N, F438W})$  chromosome map of the three clusters presented in Fig. 4: Lindsay 1 as black points in the left-hand panel, NGC 2121 as blue points in the middle panel, and NGC 1783 as red points in the right-hand panel. The histograms of  $\Delta_{F275W, F814W}$  and  $\Delta_{F275W, F343N, F438W}$  are reported in the ancillary panels, where the same colour code as for the main panels is used. Fig. 4 shows that Lindsay 1, NGC 2121, and NGC 1783 share exactly the same trend in such a parameter space, with almost the same inclination angle.<sup>3</sup> They have different extensions to each other but the observed distribution of stars of each cluster is always wider than what expected from photometric errors alone (shown in the three main panels, bottom left side). The observed spread clearly indicates the presence of MPs in the clusters, however the separation between the subpopulations looks here very small, contrary to what happens for most of the chromosome maps of MW GCs, thus preventing to distinguish between them.

The comparison of the chromosome map of the three clusters also clearly suggests that the width of the  $\Delta_{F275W, F343N, F438W}$  distribution strongly correlates with the cluster age, since it decreases going from intermediate-age clusters like Lindsay 1 to young clusters, like NGC 1783. This has been confirmed by computing the  $\Delta_{F275W, F343N, F438W}$  width for the three clusters: Lindsay 1,  $\sigma(C_{F275W, F343N, F438W})_{\text{Lindsay1}}^{\text{RGB}} = 0.12$ , NGC 2121,  $\sigma(C_{F275W, F343N, F438W})_{\text{NGC2121}}^{\text{RGB}} = 0.08$ , and NGC 1783,

<sup>2</sup> $C_{F275W, F343N, F438W} = (m_{F275W} - m_{F343N}) - (m_{F343N} - m_{F438W})$  as defined in Milone et al. (2019). It is worth to mention that for NGC 1783 we are dealing with F435W instead of F438W.

<sup>3</sup>The slope of a cluster's chromosome map slightly changes as a function of the metallicity of the cluster itself, with steeper slopes associated to more metal-poor clusters.

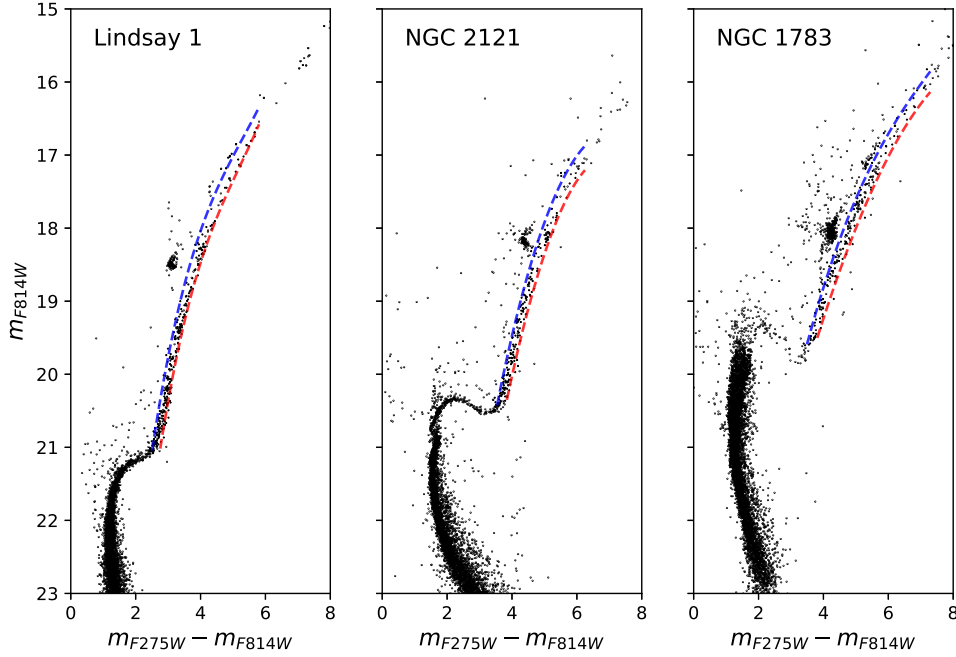


**Figure 2.**  $(m_{F814W}, m_{F275W} - m_{F814W})$  CMD for all the stars of Lindsay 1 (left-hand panel), NGC 2121 (middle panel), and NGC 1783 (right-hand panel) used in this work. Blue and red dashed lines represent the adopted fiducial lines in the analysis (see Section 3 for details).

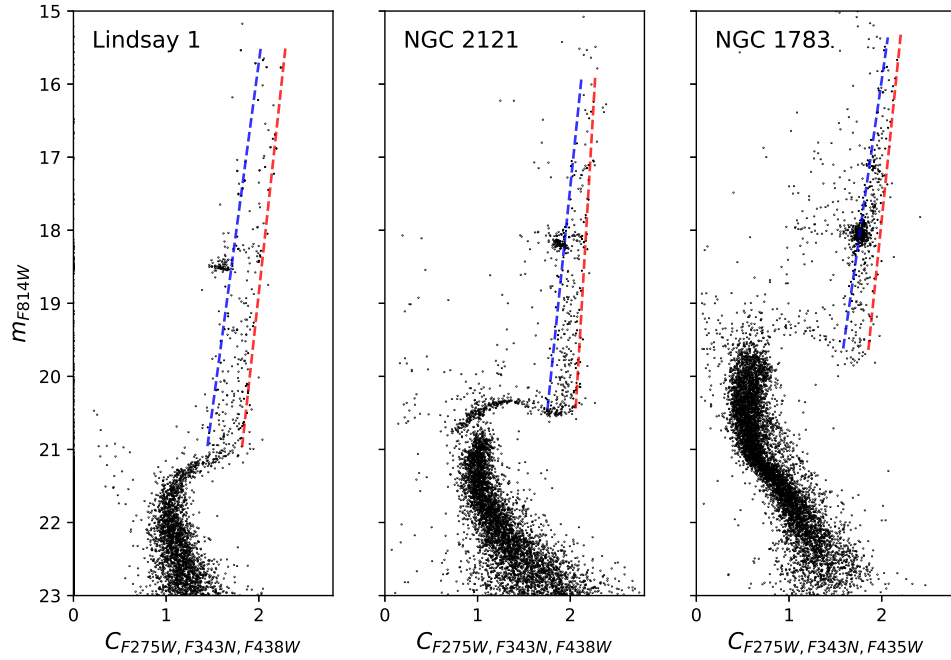


**Figure 3.**  $(m_{F814W}, C_{F275W, F343N, F435W})$  CMD for all the stars of Lindsay 1 (left-hand panel), NGC 2121 (middle panel), and NGC 1783 (right-hand panel) used in this work. Blue and red dashed lines represent the adopted fiducial lines in the analysis.

$\sigma(C_{F275W, F343N, F435W})_{\text{NGC1783}}^{\text{RGB}} = 0.06$ . This result is not unexpected since in Martocchia et al. (2019) the authors came to the same conclusion by analysing the  $\Delta_{F336W, F438W, F343N}$  and  $\Delta_{F343N, F438W, F814W}$  pseudo-colours for a much larger sample of LMC/SMC clusters.

In this regard, it is worth to mention the work by Salaris et al. (2020), where the authors have investigated the effect of the physical process called ‘first dredge-up’ on the chemical mixing (in terms of N and other light-elements) of RGB stars in star clusters, concluding that the observed  $\sigma(\Delta_{F275W, F343N, F435W})^{\text{RGB}}$  (as well

as that derived from other pseudo-colours) are always a lower limit to the real values and that the discrepancy between real versus observed widths becomes much more severe for young clusters than old/intermediate-age ones. As a direct consequence, all the N abundance spreads derived from the measured  $\sigma$  suffer from this effect, so that the results cannot be corrected in a trivial way. The effect of the first dredge-up is also visible in the pseudo-colour diagrams of Fig. 3, where the RGB width of the clusters decreases going from faint to bright magnitudes.

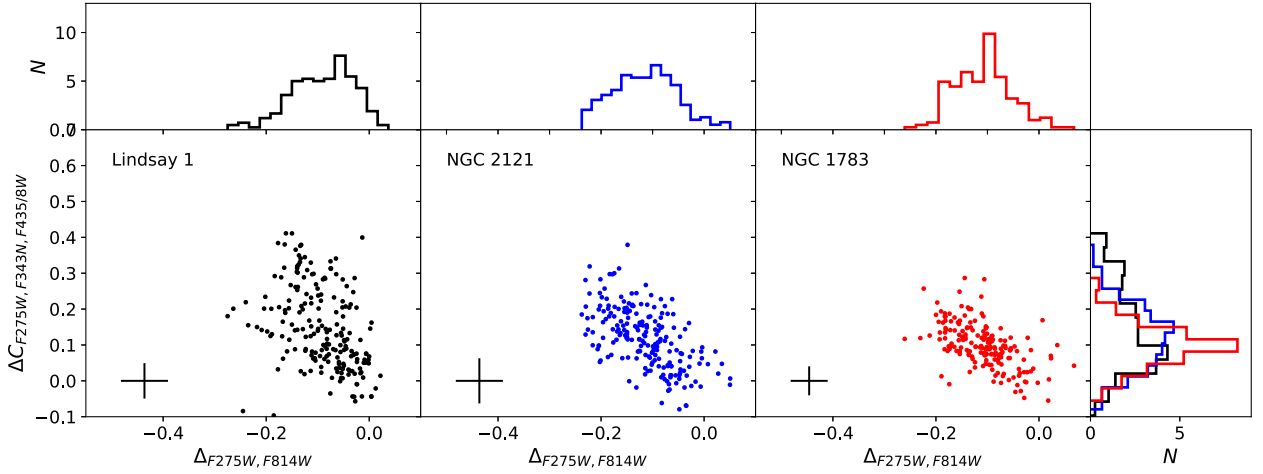


**Figure 4.** Comparison of the  $(\Delta_{F275W, F814W}, \Delta_{F275W, F343N, F435/8W})$  chromosome maps for Lindsay 1 (left, black points), NGC 2121 (middle, blue points), and NGC 1783 (right, red points). The histograms of the verticalized colour distribution  $\Delta_{F275W, F814W}$  for the three clusters are shown in the top panels, colour-coded as the main ones. In the rightmost panel instead the histograms of the verticalized pseudo-colour distribution  $\Delta_{F275W, F343N, F438W}$  for the three clusters are presented one on top of the others. A clear correlation between  $\Delta_{F275W, F343N, F438W}$  and the cluster age is visible.

In order to quantify such a variation we performed the following test: for each cluster we measured the RGB width at two different magnitude levels, the RGB base and 3 mag above this level. This choice has been made to sample the same evolutionary stage in clusters having very different ages. The comparison between these two values gives an idea of how much the RGB width varies due to the effect of the first dredge-up in each cluster. This ratio turns out to be 84.1 per cent for Lindsay 1, 66.2 per cent for NGC 2121, and 64.5 per cent for NGC 1783. As we can see, in agreement with what expected, this effect is much more evident in young clusters than in old ones, thus suggesting that the criterion used to date to normalize the RGB width (at 2 mag above the turn-off of the cluster) for deriving the chromosome maps should be in some way revised as a function of the cluster age.

#### 4 HELIUM ENRICHMENT IN NGC 2121

In a cluster hosting MPs, stars with slightly different light-element abundances (e.g. C, N, O, and Na) are expected to show also He-abundance variations. As already pointed out in the previous section, the distribution of RGB stars in the  $(m_{F275W} - m_{F814W})$  colour combination is commonly used as a tracer of such a spread since it strongly depends on the temperature. However other effects (e.g. binaries) can play a similar role in this filter combination, thus affecting in some way the results. A clear example is presented in Fig. 3 where Lindsay 1, NGC 2121, and NGC 1783 show almost the same width in the x-axis regardless their age and metal content, so that a relative comparison is not straightforward.

A better way to independently measure the He enrichment within a cluster consists in analysing the morphology of its red clump (RC) and directly comparing it with appropriate synthetic RC models, as already done for a few LMC/SMC clusters by Chantreau et al. (2019). Here we used the same method, applied to the  $(m_{F438W}, m_{F438W} - m_{F814W})$  CMD, in order to investigate the presence of an He enrichment in NGC 2121 – we refer the reader to Chantreau et al. (2019) for more details on the procedure adopted.

The RC analysis revealed that, in such an age regime, the contribution of an He enrichment ( $\Delta Y_{\text{ini}}$ ) and of a differential mass

loss on the RGB ( $\delta\eta_R$ ) of the cluster cannot be easily disentangled since they almost go in the same direction. This finding, coupled with the photometric errors of the observations ( $\sim 0.01$  mag both in magnitudes and colours), makes it difficult to draw firm conclusions about the existence of an He enrichment in NGC 2121. Indeed, an initial He spread (at fixed mass-loss) or a mass-loss spread (at fixed  $Y_{\text{ini}}$ ) can similarly approximate the colour extension and slope of the observed RC.

We found that a mass-loss parameter in the Reimers formula of about  $\eta_R = 0.38$  (corresponding to a total RGB mass-loss  $\sim 0.13 M_{\odot}$ ), is needed to fit the RC position<sup>4</sup> of NGC 2121 and if the colour extension of the RC is caused by differential mass-loss, then a total RGB mass-loss spread  $\Delta M_{\text{RGB}}$  of  $0.03\text{--}0.04 M_{\odot}$  (decreasing from  $\eta_R = 0.38$  to  $0.30$ ) would be necessary to reproduce its whole extension. To support our visual inspection, a statistical comparison between the observed and the modelled RC has been done through a 2D Kolmogorov–Smirnov (2D-KS) test. It turns out that such a range of  $\eta_R$  provides the best possible match to our observations. This is a relatively large amount considering that it roughly corresponds to the 30 per cent of the total RGB mass loss in the cluster but there is no way to rule out this scenario. It is shown in the left-hand panel of Fig. 5, where the observed RC of NGC 2121 in the  $(m_{F438W}, m_{F438W} - m_{F814W})$  CMD is compared with synthetic RC stars having  $\Delta Y_{\text{ini}} = 0$  and colour-coded as a function of the mass-loss  $\eta_R$ .

Alternatively, if we make the assumption that the mass loss along the RGB is essentially constant, which is consistent with what has been found in most stellar clusters studied so far in the MCs (Chantreau et al. 2019), then the observations are no longer compatible with models having no initial He spread. This issue can be successfully overcome by invoking a maximum He enrichment of up to  $0.020 \pm 0.005$  within NGC 2121, for a total RGB mass loss of  $\sim 0.13 M_{\odot}$ . The value of  $\Delta Y_{\text{ini}}$  suggested for NGC 2121 ( $M = 0.9 \times 10^5 M_{\odot}$ , McLaughlin & van der Marel 2005) would follow the relation observed for MW GCs and MCs

<sup>4</sup>We imposed that the reddest edge, in colour, of the synthetic RC overlaps with that of the observed RC.



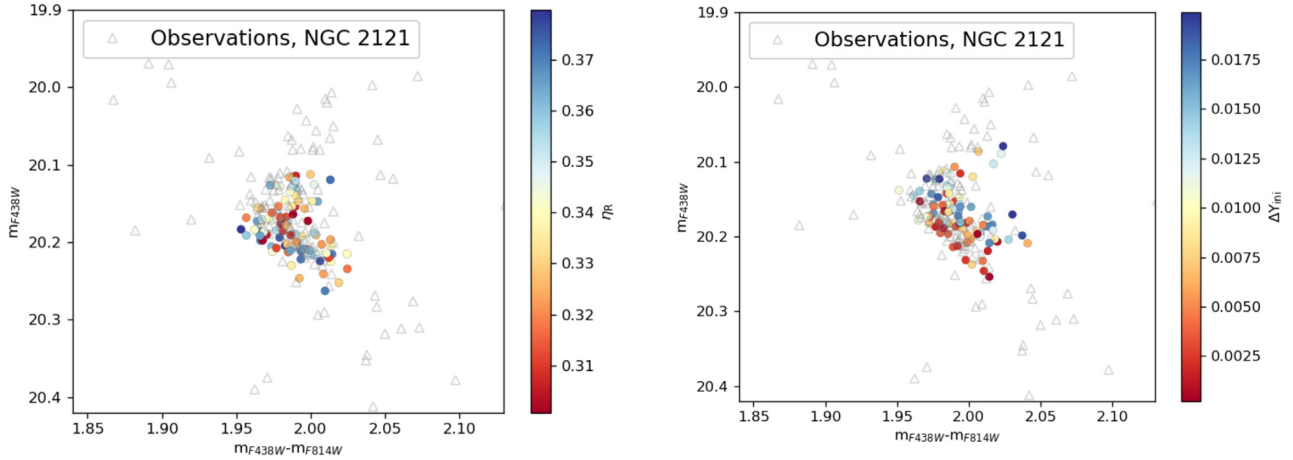


**Figure 5.** Zoom into the RC region of NGC 2121 for the  $(m_{F438W}, m_{F438W} - m_{F814W})$  CMD. The observed stars are shown as grey open triangles in both panels. Left-hand panel: synthetic RC stars with  $\Delta Y_{\text{ini}} = 0$ , colour-coded as a function of  $\eta_R$  (corresponding to a differential RGB mass-loss  $\Delta M_{\text{RGB}} \sim 0.03\text{--}0.04 M_{\odot}$ ). This model only poorly fits the full extension of the RC, thus suggesting that an initial He spread should be present within the cluster. Right-hand panel: synthetic RC stars with  $\Delta Y_{\text{ini}}$  up to 0.02 and a constant RGB mass loss of  $\sim 0.13 M_{\odot}$  are presented as filled circles, colour-coded according to the He enhancement. The RC slope and colour extension are very well reproduced here.

clusters between  $\Delta Y_{\text{ini}}$  and the mass of the cluster itself (Milone et al. 2018b; Baumgardt & Hilker 2018).

The right-hand panel of Fig. 5 shows such a case, where the observed cluster RC well overlaps with synthetic RC stars colour-coded as a function of  $\Delta Y_{\text{ini}}$ . Both the slope and the colour extension of the RC are quite well reproduced in this scenario. As before, our choice of  $\Delta Y_{\text{ini}} = 0.02$  comes from the result of a 2D-KS test: both lower and higher initial He spreads provide significantly worse matches to the data.

From a statistical point of view, the two presented scenarios are indistinguishable so that we are not able to decide which one we should prefer. We note also that the values of  $\Delta M_{\text{RGB}}$  and  $\Delta Y_{\text{ini}}$  found in this section should be considered as upper limits since a combination of these two effects (both He and mass-loss variation) can also be in place in NGC 2121.

## 5 AGE DIFFERENCE AT THE SGB LEVEL OF NGC 2121

In this section we focus on the SGB morphology of NGC 2121, in order to investigate the presence of an age difference between the two populations belonging to the cluster, with different N-abundances. To do so we follow the approach adopted by Martocchia et al. (2018b) for NGC 1778. This is an interesting aspect to look at, since the results can help to put constraints on the proposed formation mechanisms for the MPs phenomenon. Lindsay 1 and NGC 1783 have been excluded from the analysis based on their ages: Lindsay 1 is relatively old, so that the morphology of its SGB is not ideal to distinguish stars having different N-abundances, while NGC 1783 is younger than 2 Gyr, the observed age threshold for clusters hosting MPs, so that if an age difference is present, it is expected to be sensibly small.

### 5.1 SGB selection

Briefly, we first used the  $(m_{F814W}, m_{F438W} - m_{F814W})$  CMD to select the SGB stars in the colour range  $1.1 < m_{F438W} - m_{F814W} < 1.7$ , according to the red box in Fig. 6. Then we used the  $(m_{F438W},$

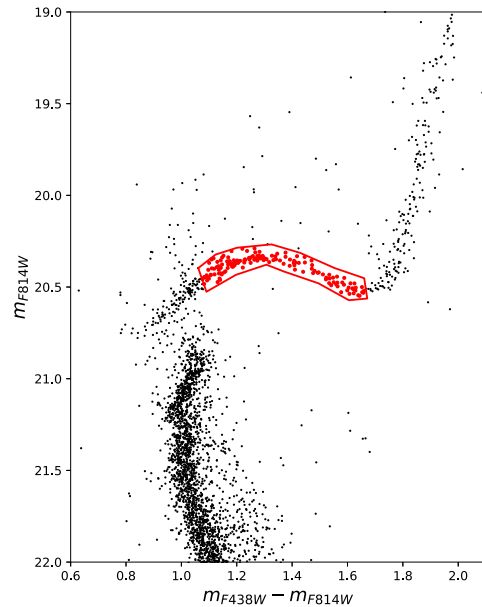


**Figure 6.**  $(m_{F814W}, m_{F438W} - m_{F814W})$  CMD of NGC 2121. The red box indicates the locus of the initial selection of SGB stars which are marked by red filled circles.

$m_{F343N} - m_{F438W})$  CMD to investigate the possible presence of a bimodal distribution for the previously selected stars. Indeed, in Martocchia et al. (2018b), the authors have demonstrated that two populations having different chemical mixtures (e.g. N-normal and N-enriched) lie in a slightly different position in the  $(m_{F438W}, m_{F343N} - m_{F438W})$  colour–magnitude space in the SGB, with the N-enriched population appearing redder than the N-normal one – refer to fig. 6 of Martocchia et al. (2018b) for more details.

The left-hand panel of Fig. 7 shows in grey the  $(m_{F438W}, m_{F343N} - m_{F438W})$  CMD of NGC 2121, while the SGB stars selected in the optical CMD and highlighted in red in Fig. 6 are superimposed here as black circles. As can be seen, in this filter combination the SGB has a peculiar shape, partially overlapping with the main sequence.

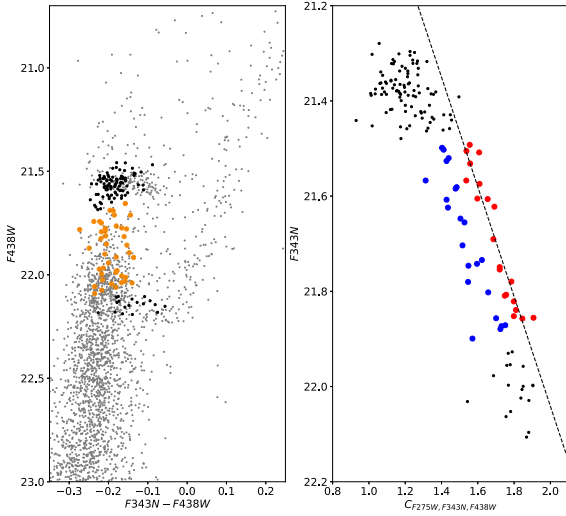


**Figure 7.** Left-hand panel: the  $(m_{F438W}, m_{F438W} - m_{F343N})$  CMD of NGC 2121 is shown in grey, with all the previously selected SGB stars overimposed as black circles. Orange filled circles represent the final selected SGB stars. Right-hand panel:  $(m_{F438W}, C_{F275W, F343N, F438W})$  pseudo-colour CMD of the first selected SGB stars (in grey) of NGC 2121. The final selected SGB stars, shown as larger circles, occupy two well-defined sequences in this diagram, one associated to a N-normal population and the other to a N-enriched one. To better visualize the two samples, we coloured them as red and blue circles, respectively. The black dashed line represent the best fit (fiducial line) of the red circles in the figure.

We then focused on the almost vertical part of the SGB, in the magnitude range  $21.6 < m_{F438W} < 22.1$ , to make the final selection of SGB stars. In this region, the observed sequence shows a hint of bimodality. The final selected SGB stars are shown as orange filled circles in Fig. 7, left-hand panel. We will call hereafter the SGB stars survived to the last selection as final SGB stars.

To properly separate the two populations, we tested once again the power of the pseudo-colour  $(C_{F275W, F343N, F438W})$ , but this time at the SGB level. This colour combination appears to work relatively well also in this case and the result is shown in the right-hand panel of Fig. 7, where the final SGB stars define two distinct sequences. The two populations have been identified and highlighted as red and blue points in the figure. It is worth to mention that, according to the definition of the pseudo-colour diagram, the  $x$ -axis is somewhat flipped so that the N-normal population lies on the red side of the diagram, while the N-enriched population on the blue one. By using the red points in Fig. 7, we defined a fiducial line for the first population (FP) as a linear best fit, which is also displayed in the figure as a black dashed line.

We then calculated the distance in  $C_{F275W, F343N, F438W}$  of each SGB star from the fiducial line to derive  $\Delta C_{F275W, F343N, F438W}$ . We fitted the rectified distribution of  $\Delta C_{F275W, F343N, F438W}$  with the Gaussian Mixture Model (GMM) in order to explore the presence of two Gaussian components in the pseudo-colour distribution. The first and second Gaussian components are shown as blue and red dashed curves, respectively, in Fig. 8 (top panel), over the histogram of  $\Delta C_{F275W, F343N, F438W}$ . The solid black line instead represents the fit of the distribution using the `SCIKIT-LEARN PYTHON` package called `MIXTURE`,<sup>5</sup> which applies the expectation-maximization algorithm for fitting mixture-of-Gaussian models. For comparison,

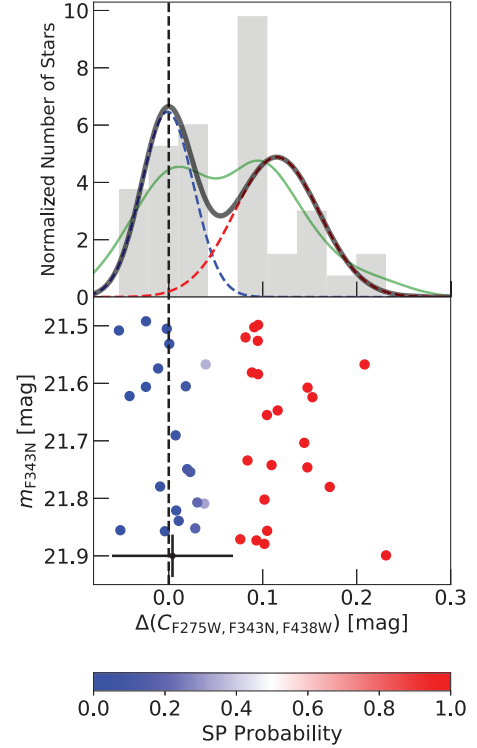


**Figure 8.** Top panel: histogram of the distribution of selected SGB stars in NGC 2121, in the  $C_{F275W, F343N, F438W}$  pseudo-colour. The black solid line represents the two-component GMM best-fitting function to the unbinned data. The blue (red) dashed curve represents the first (second) Gaussian component in the fit. The green curve indicates the KDE. Bottom panel: the  $(m_{F438W}, \Delta C_{F275W, F343N, F438W})$  pseudo-colour CMD is shown, where stars are colour-coded by the probability to belong to the SP. The black dashed line marks the adopted fiducial line. The black error bar shown in the bottom panel represents the typical error in  $C_{F275W, F343N, F438W}$  pseudo-colours and  $m_{F438W}$  magnitudes.

we also show in green the non-parametric Kernel density estimate (KDE) derived from the unbinned data. It is important to stress here that what we identified as N-normal population refers to the blue dashed curve, while the N-enriched population refers to the red dashed one. We will consider hereafter the blue component as the FP in the cluster, and the red component as the second population (SP). We assigned to each star a probability to be part of the FP and of the SP according to the results of the GMM fit. The bottom panel of Fig. 8 shows the  $\Delta C_{F275W, F343N, F438W}$  colours versus  $m_{F438W}$ , where the stars are colour-coded by the probability to be part of the SP. The adopted fiducial line is shown as a black dashed line.

## 5.2 SGB analysis

In Fig. 9 (top panel), the final SGB stars are shown in the optical  $(m_{F814W}, m_{F814W} - m_{F814W})$  CMD, where all the stars are colour-coded according to their probability (from 0 to 100 per cent) to be part of the SP in the cluster, as derived in Section 5.1. In this filter combination, the presence of chemical variations should not produce any significant spread or split in the SGB (e.g. Sbordone et al. 2011). At odds, it is well known that in optical CMDs the turn-off/SGB is the ideal region to look at for possible age differences between the FP and SP, if they are present, since their SGBs should have slightly different shapes (e.g. Li, de Grijs & Deng 2014).

<sup>5</sup><http://scikit-learn.org/stable/modules/mixture.html>

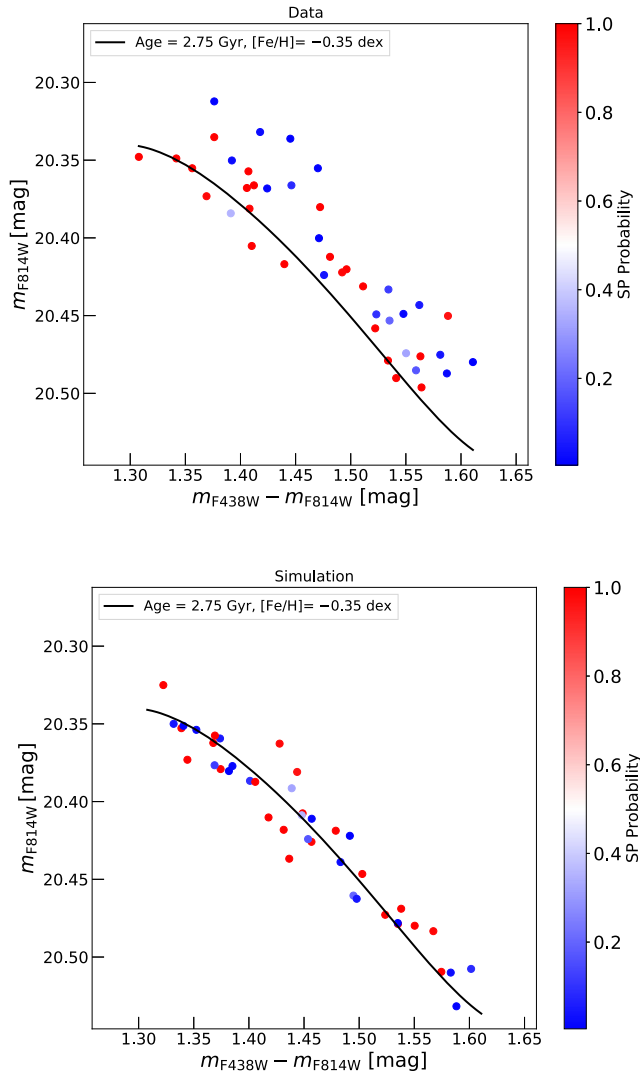


**Figure 9.** The final SGB stars in the  $(m_{F814W}, m_{F438W} - m_{F814W})$  CMD for NGC 2121 are shown in the top panel, while a Monte Carlo simulation of the SGB data, where photometric errors are taken into account, are instead presented in the bottom panel. Stars are colour-coded according to the probability to be part of the SP. The black solid line indicates the defined fiducial line of the SGB based on a BaSTI isochrone having 2.75 Gyr and  $[\text{Fe}/\text{H}] = -0.35$  dex.

In other words, if there is an age difference between the two populations of NGC 2121, we would expect a split in the optical CMD. In this section, we explore the possible presence of such a split and then estimate the age difference through comparison with isochrones at different ages.

The top panel of Fig. 9 does not show a clear offset between the populations. However, in order to address the point in a quantitative way, the idea is to compute the distance of each SGB star from a fiducial line chosen as representative of the SGB shape of the cluster, and to create from it a rectified distribution. We defined as fiducial line the SGB part of a BaSTI isochrone (Pietrinferni et al. 2004), having  $t = 2.75$  Gyr and metallicity  $[\text{Fe}/\text{H}] = -0.35$  dex. It is shown as a black solid curve in both panels of Fig. 9. The reason for using a BaSTI isochrone is the possibility to properly account for the overshooting, an effect that starts to be important in such young clusters (refer to Section 2 of Martocchia et al. 2018b for details).

We adopted both distance and reddening derived from the best fit of Martocchia et al. (2019), but we had to use a slightly older age to best match our observations. We calculated  $\Delta F814W$  as the distance in the  $F814W$  filter of each SGB star from the fiducial line. Then, we calculated the weighted mean in  $\Delta F814W$  for FP and SP stars by using the probability to be part of one of the two populations as weights. The observed age difference between the two populations, in units of magnitudes, turns out to be  $\Delta \text{Mag}_{\text{OBS}} = \Delta F814W_{\text{FP}} - \Delta F814W_{\text{SP}} = (-0.024 \pm 0.034)$  mag.

This difference in magnitude between the two populations can be easily converted in age difference in units of Myr by comparing this result with appropriate evolutionary models. As already discussed, we used BaSTI isochrones, that we interpolated from age = 2.72 to 2.79 Gyr, spaced by 10 Myr. The adopted isochrones are shown in the top panel of Fig. 10, where two vertical dashed lines indicate the selected region of the SGB used to perform the analysis. This region is exactly the one where a bimodal distribution in the pseudo-colour diagram has been identified. We first used the 2.75 Gyr isochrone as an age reference for NGC 2121. Then, we computed the mean difference in  $F814W$  magnitudes, at the SGB level, between the reference isochrone and the others (shown in Fig. 10). From these, presented as black circles in the bottom panel of Fig. 10, we derived a relation through linear fitting (red solid line) which can be used to transform the observed difference in magnitude to age difference ( $\Delta \text{Age}$ ) in Myr:

$$\Delta \text{Age}[\text{Myr}] = 2621.30 \times \Delta \text{Mag}[\text{mag}] - 0.04 \quad (1)$$

By adopting this relation, we found that the age difference in the  $(m_{F814W}, m_{F438W} - m_{F814W})$  CMD between the FP and the SP of NGC 2121 is  $-6$  Myr, with the SP slightly younger than the FP.

To estimate the uncertainty of this result, taking into account the limited number of available stars, we made use of Monte Carlo simulations. Starting from a single isochrone model, we simulated a sample having the same number of stars as the ones previously adopted, we added their photometric errors and we assigned to each of these stars the same probability distribution of belonging to the FP and the SP as in the real data. We repeated this process 100 000 times to be statistically robust. One of these simulations is reported, as an example, in the bottom panel of Fig. 9 and as can be seen, it reproduces pretty well the observations. For each simulation, we calculated the simulated  $\Delta F814W$  for each population and thus  $\Delta \text{Mag}_{\text{OBS}}$ . We found that the Monte Carlo distribution has a mean of 0 mag, as expected, and  $\sigma = 0.0046$  mag, which translates into an age difference of 12 Myr, computed using equation (1).

We found that the age difference between the two populations in the SGB of NGC 2121 is then  $-6 \pm 12$  Myr, which is consistent with no age spread. In order to be sure that an error in the determination of the best-fitting age of the cluster does not affect our conclusions, we took ages of 2.0 and 3.0 Gyr as reference to do the same exercise. In the first case, we found an age difference between FP and SP of  $-4.6 \pm 6$  Myr, while in the second one, the age difference turned out to be of  $-8 \pm 14$  Myr. Both results confirm that the observed difference in age between the two populations of NGC 2121 is small and consistent with zero, regardless the isochrone used to make such an estimate.

It is worth to mention that star-to-star variations of He abundance might also generate an offset on the SGB (Kim & Lee 2018). At these ages, in particular, the SGB of an He-enriched population appears slightly fainter than the SGB of an He-normal population, thus contributing to compensate in some way the effect of an age difference between the two. In order to quantify the impact of an He

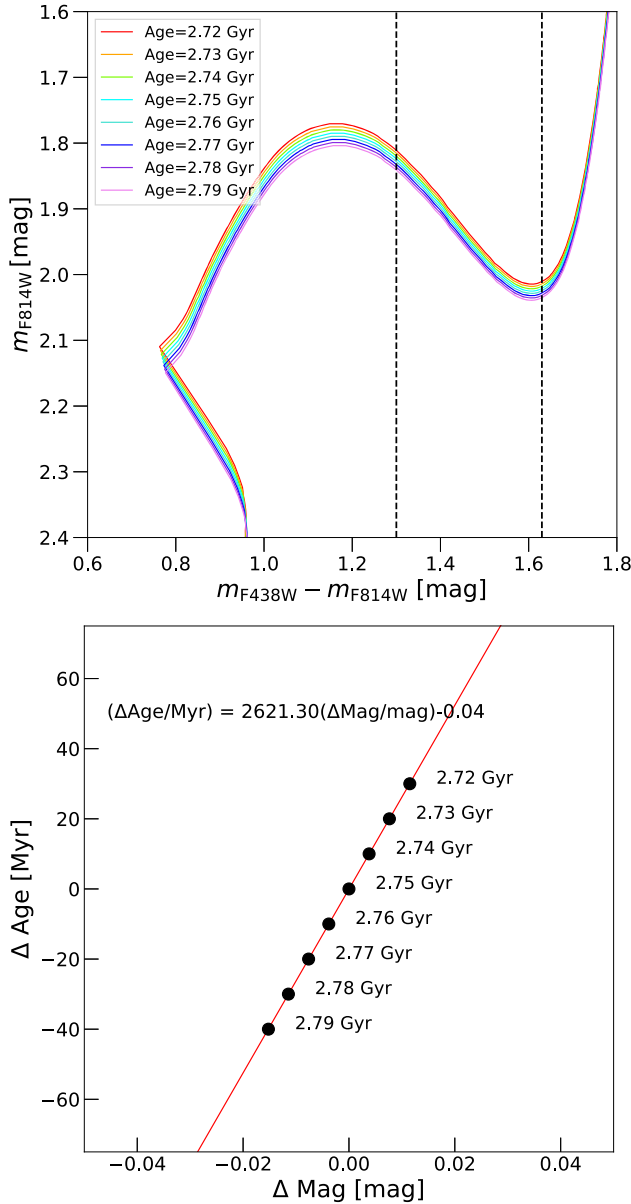


**Figure 10.** Top panel: BaSTI isochrones in the  $(m_{F814W}, m_{F438W} - m_{F814W})$  CMD with ages spanning a range from 2.72 up to 2.79 Gyr, spaced by 10 Myr ( $[\text{Fe}/\text{H}] = -0.35$  dex). The vertical black dashed lines define the portion of the SGB used to compute the difference in age between the two populations. Bottom panel: the relation between  $\Delta \text{Mag}$  and  $\Delta \text{Age}$  for the SGB is presented as a solid red. The black circles indicate the values obtained for the isochrones shown in the top panel. See the text for more details on the procedure.

spread on the SGB analysis, we compared two isochrones from the Victoria–Regina stellar models (Casagrande & VandenBerg 2014), having age and metallicity of NGC 2121 but a slightly different He content ( $Y = 0.256$  for the He-normal population and  $Y = 0.276$  for the He-enriched one), following what have been derived in Section 4. We found that the isochrones are indistinguishable in the SGB portion ( $1.3 < m_{F438W} - m_{F814W} < 1.65$ ; see Fig. 10, top panel) we used to compute the age differences between the two populations, so that the presence of a possible He spread does not have any impact on our estimate of  $\Delta \text{Age}_{P1 - P2}$ .

## 6 DISCUSSION AND CONCLUSIONS

In this work, we made use of high-resolution near-UV/optical archival and proprietary *HST* observations to study in detail the presence of MPs in the LMC clusters NGC 2121 and NGC 1783, having ages of  $\sim 2.5$  and  $\sim 1.5$  Gyr, respectively. In particular we exploited the power of the F343N filter to create an alternative ‘chromosome map’ (Milone et al. 2017), which is able to efficiently separate subpopulations of stars having different N-abundances. By comparing these chromosome maps with that of the intermediate-age ( $\sim 7.5$  Gyr) cluster Lindsay 1 (Saracino et al. 2019b), we found a clear correlation between the width ( $\sigma$ ) of the  $\Delta F_{275W, F343N, F438W}$  distribution and the age of the cluster itself, with larger  $\sigma$  associated to older ages. This finding well agrees with the results found by Martocchia et al. (2019, and references therein) on a large sample of LMC/SMC clusters. However, this no longer implies that the N-enhancement within a cluster decreases going from old to young ages because of the effect of the first dredge-up which modifies the observed  $\Delta F_{275W, F343N, F438W}$  in a not straightforward way (Salaris et al. 2020).

The construction of chromosome maps for clusters belonging to (non-accreted) galaxies outside the MW has been recently possible (Saracino et al. 2019b; Sills et al. 2019; Milone et al. 2019 show few examples). This is a very good opportunity since the one-to-one comparison allows to show up possible similarities and/or differences among clusters belonging to galaxies having different morphologies and star formation histories. In this respect, what already found by Saracino et al. (2019b) and here confirmed for NGC 2121 and NGC 1783 is that, in the chromosome maps of LMC/SMC clusters, the N-normal and N-enriched populations appear to follow a rather continuous sequence, instead of creating two well-separated clumps, as many MW GCs do. At odds, all of them occupy the same parameter space, with almost the same shape as MW GCs. This finding, if further observed in other LMC/SMC clusters, could open to new and still unexplored questions.

Since these clusters have different metallicities, it would be then interesting to compare them in a metallicity-free parameter space. However, the metallicity-dependent corrections used by Marino et al. (2019) to create a ‘universal’ chromosome map and tested by Sills et al. (2019) on the Sagittarius dwarf cluster M54, only work for clusters where the position of the FP can be easily determined. It is not the case for LMC/SMC clusters.

Finally, we focused a bit more in detail on NGC 2121, by exploring two main features: (1) the RC morphology, in order to infer the He enrichment of the cluster; and (2) the structure of the SGB, in order to investigate whether the N-normal and N-enriched populations show different ages.

The RC study of NGC 2121 revealed that the effects of an He enrichment and a differential mass loss along the RGB are somehow coupled for clusters having such an age and metallicity. Indeed, two possible scenarios can most likely take place in such a cluster: (1)  $\Delta Y_{\text{ini}} = 0.0$  and  $\Delta M_{\text{RGB}} = 0.03\text{--}0.04$ ; and (2)  $\Delta Y_{\text{ini}} = 0.020 \pm 0.005$  and  $\Delta M_{\text{RGB}} = 0.0$ .

We cannot give a firm answer to which one should be preferred since they are statistically indistinguishable, but we can consider these values as upper limits since a combination of these two effects could also be in place in NGC 2121.

From the SGB analysis, we found that  $C_{F275W, F343N, F438W}$  is a powerful pseudo-colour to identify FP and SP even at the SGB level, thus allowing to easily distinguish between them. By using the optical  $(m_{F814W}, m_{F438W} - m_{F814W})$  CMD we then derived an age difference of  $-6 \pm 12$  Myr, which is relatively small (with the



SP slightly younger than the FP), and consistent with zero within the uncertainties. This result turns out to be in very good agreement with what found in the  $\sim 2$  Gyr old LMC star cluster NGC 1978 by Martocchia et al. (2018b), the only other cluster where such a test has been possible, thus strengthening the constraints on the onset of MPs and on the source of the chemical enrichment within clusters. Indeed, theories predicting an age difference from at least 30 up to 200 Myr between the FP and SP appear to be ruled out from such experiments. Further theoretical efforts seem to be required in order to explain all the recent findings in the context of a general framework.

## ACKNOWLEDGEMENTS

We acknowledge the anonymous referee for the detailed review and helpful suggestions, which allowed us to improve the manuscript. SS and NB gratefully acknowledge financial support from the European Research Council (ERC-CoG-646928, Multi-Pop). NB also acknowledges support from the Royal Society (University Research Fellowship). WC acknowledges funding from the Swiss National Science Foundation under grant P2GEP2 171971. VK-P is very grateful to Jay Anderson for sharing with us his ePSF code. CL thanks the Swiss National Science Foundation for supporting this research through the Ambizione grant number PZ00P2 168065. The authors gratefully acknowledge financial support for programs GO-14069, GO-15062, and GO-15630, provided by NASA through Hubble Fellowship grant HST-HF2-51387.001-A awarded by the Space Telescope Science Institute, which is operated by the Association of Universities for Research in Astronomy, Inc., for NASA, under contract NAS5-26555.

## REFERENCES

- Bastian N., Lardo C., 2018, *A&A*, 56, 83  
 Baumgardt H., Hilker M., 2018, *MNRAS*, 478, 1520  
 Bragaglia A., Gratton R. G., Carretta E., D’Orazi V., Sneden C., Lucatello S., 2012, *A&A*, 548, A122  
 Cabrera-Ziri I. et al., 2016, *MNRAS*, 459, 4218  
 Cardelli J. A., Clayton G. C., Mathis J. S., 1989, in Allamandola L. J., Tielens A. G. G. M., eds, IAU Symp. Vol. 135, Interstellar Dust. Kluwer, Dordrecht, p. 5  
 Carretta E., Bragaglia A., Gratton R. G., Recio-Blanco A., Lucatello S., D’Orazi V., Cassisi S., 2010, *A&A*, 516, A55  
 Casagrande L., Vandenberg D. A., 2014, *MNRAS*, 444, 392  
 Chantreau W., Salaris M., Bastian N., Martocchia S., 2019, *MNRAS*, 484, 5236  
 Conroy C., Spergel D. N., 2011, *ApJ*, 726, 36  
 D’Ercole A., Vesperini E., D’Antona F., McMillan S. L. W., Recchi S., 2008, *MNRAS*, 391, 825  
 Dalessandro E. et al., 2018, *A&A*, 618, A131  
 Dalessandro E., Lapenna E., Mucciarelli A., Origlia L., Ferraro F. R., Lanzoni B., 2016, *ApJ*, 829, 77  
 Dalessandro E., Ferraro F. R., Bastian N., Cadelano M., Lanzoni B., Raso S., 2019, *A&A*, 621, A45  
 Decressin T., Meynet G., Charbonnel C., Prantzos N., Ekström S., 2007, *A&A*, 464, 1029  
 Denissenkov P. A., Hartwick F. D. A., 2014, *MNRAS*, 437, L21  
 Ferraro F. R., Possenti A., Sabbi E., Lagani P., Rood R. T., D’Amico N., Origlia L., 2003, *ApJ*, 595, 179  
 Gaia Collaboration et al., 2016, *A&A*, 595, A2  
 Gaia Collaboration et al., 2018, *A&A*, 616, A1  
 Gieles M. et al., 2018, *MNRAS*, 478, 2461  
 Gilligan C. K. et al., 2019, *MNRAS*, 486, 5581  
 Glatt K. et al., 2008, *AJ*, 136, 1703  
 Hollyhead K. et al., 2017, *MNRAS*, 465, L39  
 Kim J. J., Lee Y.-W., 2018, *ApJ*, 869, 35  
 Lanzoni B., Dalessandro E., Ferraro F. R., Miocchi P., Valenti E., Rood R. T., 2007, *ApJ*, 668, L139  
 Larsen S. S., Brodie J. P., Grundahl F., Strader J., 2014, *ApJ*, 797, 15  
 Li C., de Grijs R., 2019, *ApJ*, 876, 94  
 Li C., de Grijs R., Deng L., 2014, *Nature*, 516, 367  
 Marino A. F. et al., 2012, *ApJ*, 746, 14  
 Marino A. F. et al., 2019, *MNRAS*, 487, 3815  
 Martocchia S. et al., 2017, *MNRAS*, 468, 3150  
 Martocchia S. et al., 2018a, *MNRAS*, 473, 2688  
 Martocchia S. et al., 2018b, *MNRAS*, 477, 4696  
 Martocchia S. et al., 2019, *MNRAS*, 487, 5324  
 McLaughlin D. E., van der Marel R. P., 2005, *ApJS*, 161, 304  
 Milone A. P. et al., 2012, *A&A*, 540, A16  
 Milone A. P. et al., 2015, *MNRAS*, 447, 927  
 Milone A. P. et al., 2017, *MNRAS*, 464, 3636  
 Milone A. P. et al., 2018a, *MNRAS*, 477, 2640  
 Milone A. P. et al., 2018b, *MNRAS*, 481, 5098  
 Milone A. P. et al., 2019, *MNRAS*, 491, 515  
 Milone A. P., Bedin L. R., Piotto G., Anderson J., 2009, *A&A*, 497, 755  
 Moffat A. F. J., 1969, *A&A*, 3, 455  
 Montegriffo P., Ferraro F. R., Fusi Pecci F., Origlia L., 1995, *MNRAS*, 276, 739  
 Mucciarelli A., Origlia L., Ferraro F. R., 2007, *AJ*, 134, 1813  
 Mucciarelli A., Origlia L., Ferraro F. R., Pancino E., 2009, *ApJ*, 695, L134  
 Nardiello D. et al., 2015, *MNRAS*, 451, 312  
 Nardiello D. et al., 2018, *MNRAS*, 481, 3382  
 Niederhofer F. et al., 2017a, *MNRAS*, 464, 94  
 Niederhofer F. et al., 2017b, *MNRAS*, 465, 4159  
 Pietrinferni A., Cassisi S., Salaris M., Castelli F., 2004, *ApJ*, 612, 168  
 Piotto G. et al., 2015, *AJ*, 149, 91  
 Salaris M. et al., 2020, *MNRAS*, 492, 3459  
 Saracino S. et al., 2019a, *MNRAS*, 489, L97  
 Saracino S. et al., 2019b, *ApJ*, 874, 86  
 Sbordone L., Salaris M., Weiss A., Cassisi S., 2011, *A&A*, 534, A9  
 Schiavon R. P., Caldwell N., Conroy C., Graves G. J., Strader J., MacArthur L. A., Courteau S., Harding P., 2013, *ApJ*, 776, L7  
 Sills A., Dalessandro E., Cadelano M., Alfaro-Cuello M., Kruijssen J. M. D., 2019, *MNRAS*, 490, L67  
 Stetson P. B., 1987, *PASP*, 99, 191  
 Stetson P. B., 1994, *PASP*, 106, 250  
 Zhang H., de Grijs R., Li C., Wu X., 2018, *ApJ*, 853, 186

This paper has been typeset from a  $\text{\LaTeX}$  file prepared by the author.